Engineered Science
DOI: https://dx.doi.org/10.30919/es1782

Plasmon Effect of Silver Nanoparticles on the Sensitization of Titanium Dioxide Nanorods with N719 Dye

G. Omarova,[1,*] A. Sadykova,[1] T. Serikov,[1,*] E. Seliverstova,[1] N. Ibrayev[1] and N. Nuraje[2,3]

Abstract

The plasmon effect of Ag nanoparticles (NPs) on the sensitization of TiO_2 nanorods (NRs) with ruthenium dye N719 was studied. TiO_2 NRs were prepared by hydrothermal method. SEM analysis revealed that the synthesis resulted in the formation of TiO_2 NRs with a length of ~2.6 μm and a diameter of 55 – 65 nm. The diameter of the deposited Ag NPs ranges from 5 to 12 nm. Measurements of the kinetics of fluorescence and long-lived luminescence of the dye showed that the lifetime of both types of N719 luminescence is reduced by ~2.2 times in the presence of semiconductor. At the same time, along with the dye fluorescence (near the 535 nm), a broad luminescence band at 720 nm was recorded, corresponding to the recombination luminescence of TiO_2. The results obtained indicate the electron transfer from both singlet- and triplet-excited dye molecules to TiO_2. The charge transfer efficiency was also evaluated from photovoltaic measurements of dye-sensitized solar cells (DSSC) based on TiO_2 NRs with different concentrations of Ag NPs. The best photovoltaic parameters were registered for the sample of TiO_2 NRs with Ag NPs, obtained from 1.5 mmol of $AgNO_3$. In these samples the efficiency of the solar cell was increased by 3.2 times compared to the sample without Ag NPs. The increase in efficiency is associated with the improvement of charge transport characteristics of solar cells with Ag NPs, which was confirmed by impedance measurements. The injection of hot electrons from Ag NPs into the TiO_2 conduction band is also possible, which contributes to the enhancement of solar cell efficiency. The obtained data demonstrate the potential of using of plasmon effect of metal NPs to enhance the efficiency of DSSCs and could be applied in the design of high-performance photovoltaic systems.

Keywords: TiO_2 nanorods; Ag nanoparticles; Electron transfer; Dye N719; DSSC.
Received: 08 August 2025; Revised: 26 September 2025; Accepted: 02 October 2025
Article type: Research article.

1. Introduction

Among third-generation solar cells, dye-sensitized solar cells (DSSCs) are one of the most extensively studied and have attracted considerable research attention over the past fifteen years. According to the search results with the "DSSC" word an approximately one thousand annual publications are displayed, which confirms the relevance of this area. The main advantages of DSSCs are their simplicity of manufacture, the possibility of assembling of flexible elements, the using of inexpensive components, and theoretically high efficiency.[1-3] At the moment, the efficiency of conversation of solar radiation into electricity with DSSC is lower than for the best thin-film cells, but the theoretical calculated price-performance ratio can compete with traditional energy sources.[4]

As is well known, in DSSC cells, dye molecules absorb photons and transfer electrons to the conduction band of the semiconductor, from where charge carriers diffuse to the counter electrode. The oxidized dye is reduced by the electrolyte.[5] Cell efficiency is determined by the balance between electron injection from the dye to the semiconductor and competing recombination processes.[6,7]

Significant progress in improving the efficiency and stability of DSSCs can be achieved primarily through the optimization of charge transfer processes.[8] Therefore, the issue of photoinduced interfacial charge transfer at the "semiconductor–dye" interface has attracted considerable

[1]*Institute of Molecular Nanophotonics, Buketov Karaganda University, Karaganda, 100024, Kazakhstan*
[2]*Department of Chemical and Materials Engineering, School of Engineering and Digital Science, Nazarbayev University, Astana, 010000, Kazakhstan*
[3]*Renewable Energy Laboratory, National Laboratory Astana, Nazarbayev University, Astana, 010000, Kazakhstan*
[*]*Email :* imnph@mail.ksu.kz (G. Omarova), serikov-timur@mail.ru (T. Serikov)

research interest. The rates of charge transfer and recombination processes largely depend on the energy level alignment at the interface of the used materials, their morphology, preparation conditions, and chemical interactions.[9] Generally, metal oxides like TiO_2, SnO_2 and ZnO are often used as semiconductors in DSSC cells due to their suitable band gap width (3.0 – 3.6 eV), the ability to control their properties by selecting the synthesis method and conditions, optical transparency, and developed specific surface area.[10-14] At the same time, the most widespread use in DSSCs is an array of randomly distributed spherical TiO_2 nanoparticles with a layer thickness of ~10 μm.[15] However, unformed bonds between particles and grain disorder lead to reduced mobility of charge carriers, their slow transport and recombination in semiconductor films.[16,17] In order to eliminate these shortcomings, DSSCs can use one-dimensional nanostructured semiconductor photoanodes, such as nanorods,[18] nanotubes[19] and nanosheets[20] of semiconductors, which demonstrate superior charge transfer properties.[21] It should be noted that the highest solar cell efficiencies (around 12%) were achieved for TiO_2 nanostructures using ruthenium pyridylthiocyanate complexes with various substituents in the pyridine molecules, in particular, dyes N3, N749 and N719.[22,23] Subsequently, using alkoxysilyl- and carboxy-anchored organic dyes, the efficiency of DSSCs was increased to 14%.[24] The authors indicate that the increase in efficiency is mainly associated with improved light-harvesting and charge-transport characteristics of working electrodes based on TiO_2 nanostructures. Nevertheless, the efficiency of DSSCs remains low compared to theoretical calculations, so over the past few years, attempts have been made to improve the efficiency of solar cells using various dyes,[25,26] semiconductors of different morphologies and metal nanoparticles,[27,28] quantum dots,[29,30] active layers of various morphologies[31,32] and new electrolytes.[33] Among the approaches mentioned, the most promising one seems to be the using of plasmon metal nanoparticles (NPs) in the working electrode.

Localised surface plasmon resonance (LSPR) of metal NPs leads to improved optical absorption, generation of charge carriers and overall efficiency of conversation of solar radiation into electricity.[34,35] Among NPs with LSPR, silver NPs demonstrate the highest plasmonic properties.[36-41] In Ref.[42] the photovoltaic characteristics of DSSC were analyzed in detail, which depended on size of Ag NPs. It was found that the efficiency of the solar cell was increased by 45%. In addition, the authors of Ref.[43] studied the effect of embedding of Ag NPs into the TiO_2 and their influence on the photoelectric characteristics of DSSCs. Structural and optical analyses confirmed that Ag NPs increase light harvesting due to plasmon effects, improved charge transfer and reduced electron-hole recombination. Also, the presence of Ag NPs in TiO_2 can lower the specific electrical resistance of thin composite films and shifts its absorption to the visible and IR ranges of the spectrum when the chlorophyll was adsorbed on them.[44] Moreover, at a concentration of Ag NPs up to 45 mol%, the electrode exhibits n-type conductivity, while a further increase in concentration led to a change in the conductivity of the electrode, which made it possible to create an electrode with p-type conductivity. The resulting enhancement of the photoelectric activity of the cell can be explained by the fact that the Z-scheme obtained in the photocathode enhances the separation, diffusion and transformation of electron/hole pairs within the structure. A heterojunction built according to the Z-scheme creates a path that effectively separates these electron-hole pairs, preventing their recombination and promoting the directed movement of these charge carriers to designated reaction sites within the photocathode. By ensuring a higher concentration of separated electrons and holes, the use of a Z-scheme allows for more efficient conversion of light energy into electrical energy. The presence of Ag NPs reduces electron transfer and increases recombination times.[45] Similar work was carried out for different TiO_2 structures. For example, it was shown that the charge transfer resistance and light-harvesting was reduce, as the increased efficiency of DSSC to 4.15% in the hierarchically structured TiO_2 nanorods with Ag NPs deposited by photoreduction method, the absorption capacity of the material was significantly improved.[46]

Despite the above-mentioned studies, the problem of the influence of plasmonic NPs and their concentration on the characteristics of DSSCs based on TiO_2 nanorods (NRs) and N719 dye remains open. In addition, in published works, the influence of Ag NPs on DSSC efficiency was mainly evaluated using impedance spectroscopy, stationary voltammetry, and photometry methods. In addition to the above methods, in present work fluorescence spectroscopy and time-correlated single photon counting were used, which will provide additional information about the dynamics of charge carrier transport from the dye to the semiconductor.

2. Experimental section

2.1 Materials

Major part of chemical reagents and materials used in this work were purchased from Sigma–Aldrich, including: titanium butylate $C_{16}H_{36}O_4Ti$ (97%), titanium tetraisopropoxide (TTIP, 99.999%), silver nitrate ($AgNO_3$,

99.998%), sodium borohydride ($NaBH_4$, 98%), FTO glass substrates (fluorine tin oxide, 7 Ω/cm^2), N719 dye (di-tetrabutylammonium cis-bis(isothiocyanato)bis(2.2'-bipyridyl-4.4'-dicarboxylato) ruthenium (II), 95%), polyvinylpyrrolidone (PVP, M_w=40 000, 99%), hydrochloric acid (HCl, 36.5%), nitrogen (anhydrous, 11.5–12.8%), H_2PtCl_6 (99.9%). Iodolyte H30 and Meltonix film were purchased from Solaronix.

2.2 Material preparation

2.2.1 Synthesis of NRs

TiO_2 NRs were obtained by hydrothermal synthesis according to the method described in the Ref.[47] Briefly, FTO-coated glass substrates were pre-cleaned in an ultrasonic bath in a mixture of deionized water, acetone and 2-propanol (1:1:1 volume ratio) for 30 minutes. Then, the substrates were placed by conductive side down in an autoclave filled with 35 mL of deionized water, 35 mL of HCl and 0.35 mL of titanium butylate. Next, the autoclave was placed in an oven and kept at a temperature of 160°C for 6 hours. The autoclave was then cooled to room temperature in a natural environment. The resulting films of TiO_2 NRs were washed with isopropanol, then with deionized water, and calcined at 500°C for 2 hours.

2.2.2 Synthesis of Ag NPs

To obtain Ag NPs on the surface of TiO_2 NRs, chemical deposition was used.[48] For this purpose, 0.2 g of PVP was dissolved in 40 mL of H_2O and $C_2H_6O_2$ (1:1 by volume) and 0.2 mg of $NaBH_4$ was added upon vigorous stirring. The resulting mixture was mixed for about 5 minutes. Substrates with TiO_2 NRs were immersed into the prepared solution. Then, the required amount of $AgNO_3$ was added and the vessel was kept in an oven at 70°C for 2 minutes. The concentration of Ag NPs deposited on the surface of TiO_2 NRs was varied by changing the molar mass of added $AgNO_3$: 0.5, 0.75, 1.0, 1.5, and 2.0 mmol. Accordingly, samples of NRs with different concentrations of Ag NPs are designated as TAg_0.5, TAg_0.75, TAg_1.0, TAg_1.5, and TAg_2.0, respectively. Then, the sample was washed with deionized water and dried at room temperature. The chemical reaction of silver reduction under these conditions is as follows Eq. (1):

$$2AgNO_3 + 2NaBH_4 \rightarrow 2Ag + H_2\uparrow + B_2H_6 + 2NaNO_3 \quad (1)$$

2.3 Assembly of DSSC

To assemble the DSSCs, the films obtained in section 2.2 were used. N719 ruthenium dye was deposited onto the TiO_2 surface by adsorption from an ethanol solution. The dye concentration in solutions was 10^{-4} mol/L. After complete drying, the samples were washed with an equal amount of ethanol. Platinum films for the counter electrodes was deposited on FTO from an ethanol solution of H_2PtCl_6 using an electrochemical method. FTO substrates were sequentially cleaned using detergent, deionized water, acetone, and 2-propanol for 1 hour using an ultrasonic bath. The substrates were then heated to 90°C for 30 minutes to completely remove the organic cleaning agents. Electrochemical deposition of Pt was carried out in a standard three-electrode cell using FTO-coated glass as the working electrode, a Ag/AgCl electrode as the reference, and a graphite rod as the counter electrode. Aqueous solution of H_2PtCl_6 (10 mM) with KCl (10 mM) as the supporting electrolyte was used. Platinum was deposited at –0.5 V (vs. SCE) for 5 min at room temperature, resulting in a uniform Pt layer on the FTO surface. The electrochemical deposition process ensures uniform Pt coverage and enables precise control of the film thickness by adjusting the applied potential and deposition time. This step is critical, as the film thickness directly affects light absorption and charge transfer from the electrolyte to the dye: an overly thin film reduces catalytic activity and hinders dye regeneration, whereas an excessively thick film decreases conductivity, light transmittance, and charge-transport properties.

Next, the electrodes obtained were sealed with 30 μm Meltonix film (Solaronix). Iodolyte H30 (Solaronix) was used as the electrolyte in the DSSCs, which was poured between two sealed electrodes through a pre-made hole that was subsequently hermetically sealed.

2.4 Materials characterization

The surface morphology of TiO_2 NRs and films with Ag NPs was studied using a Mira 3LMU scanning electron microscope (SEM, Tescan). To obtain information about the elemental composition of the received samples an energy dispersive analysis (EDA, Oxford Instruments) was used. The phase composition of the samples was studied using X-ray diffraction (XRD, Rigaku) with a CuKα radiation source, λ=1.54060 Å. The diffraction pattern was analyzed and the phases were identified using a database and the standard WinXPow software package. The sizes of the synthesized Ag NPs were evaluated by dynamic light scattering method (S90 analyzer, Malvern).

Absorption spectra were registered with Cary 300 spectrophotometer (Agilent). Photoluminescence spectra of the samples were recorded on Eclipse spectrofluorometer (Agilent). The samples were placed in an Optistat DN optical cryostat (Oxford Instr.) and evacuated to a residual pressure of $8 \cdot 10^{-2}$ mbar. The long-lived luminescence decay kinetics were recorded with an FLS1000 spectrometer (Edinburgh Instr.).

The fluorescence lifetimes were determined using a time-correlated single photon counting system (TCSPC, Becker&Hickl) at an excitation wavelength of λ_{exc} = 532 nm. The fluorescence lifetime was estimated from the SPCImage software (Becker&Hickl), where the intensity of luminescence

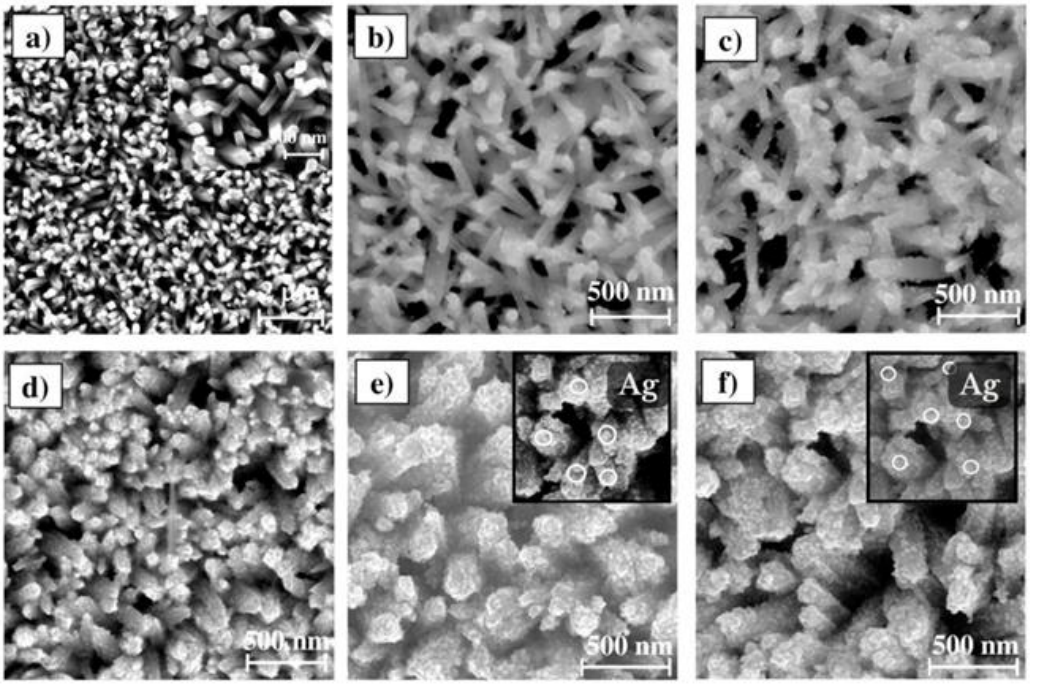

Fig. 1: SEM images of the surface of TiO_2 NRs before and after deposition of Ag NPs: a) TiO_2 NRs; b) TAg _0.5; c) TAg_0.75; d) TAg_1.0; e) TAg_1.5; f) TAg_2.0. In the inset – increased part of TEM images of TiO_2 NRs with Ag NPs.

decay was described by the Eq. (2):

$$I(t) = \sum_{i=1}^{n} \alpha_i \exp(-t/\tau_i) \quad (2)$$

where τ_i is the lifetime, α_i is an amplitude or contribution of the i-th component ($\sum_i \alpha_i = 1.0$).

The photovoltaic parameters of DSSCs were measured using a CT50AAA solar radiation simulator (PET, Photo Emission Tech. Inc.) equipped with a 100 mW/ cm^2 Xe lamp with an AM 1.5 filter. Impedance spectroscopy was used to analyze the electrophysical characteristics of the samples. Data were taken in the frequency range from 1 MHz to 100 MHz on a potentiostat with an EIS analyser (CS350, Corrtest Instruments).

3. Results and discussion

SEM images of the surface morphology of TiO_2 films with and without deposited Ag NPs are shown at Fig. 1. It is seen that TiO_2 NRs have a predominantly perpendicular orientation relative to the substrate plane.

The average length of TiO_2 NRs is ~2.6 μm with an average diameter of 55 – 65 nm. As a result of chemical reduction of silver nitrate with sodium borohydride, spherical Ag NPs are formed on the surface of the NRs (Fig. 1b). According to the SEM data, the average size of Ag NPs varies from 7 to 25 nm. With increasing of $AgNO_3$ concentration, a growth in the number of silver NPs on the surface of TiO_2 NRs is observed (Fig. 1(c – f)). The difference between the Ag NPs sizes determined from SEM images and the values obtained from DLS data (fig. 1 and 3b) is due to the difference in measurement conditions. The SEM images show NPs in an adsorbed state on the TiO_2 surface, where partial aggregation is possible, which visually increases the size of the observed objects. Meanwhile, the data obtained from optical measurements and calculations reflect the average effective size of dispersed Ag NPs in solution. Thus, the discrepancy in values is due to both the aggregation of NPs on the surface during sample preparation for SEM and the difference in measurement techniques.

EDA showed (Fig. 2) that the samples contain O and Ti patterns, which correspond to TiO_2 NRs. Also, the sample contains Sn, Ca, Na, and Cl atoms (within the margin of error), which corresponds to the composition of the glass substrate and the FTO conductive coating.

In the EDA spectra of TAg samples, an Ag patterns is also visible along with the patterns described above (Fig. 2 (b – f)). At the same time, the amount of Ag increases with increasing NPs concentration from 1.9% for the TAg_0.5 sample to 6.8% for TAg_2.0.

The XRD spectra of the TiO2 NRs have shown (Fig. 3a) the main reflections corresponded to the tetragonal modification of rutile (27.4°, 36.1°, 41.3°, 54.4°, 56.53°, 62.9° and 69.9°) that are indicated by (110), (101), (200), (111), (210), (211), (002), (310) and (301) Miller indexes, respectively (JCPDS, No. 21–1276, rutile). When Ag NPs were deposited, characteristic peaks of Ag appear at 38.11°, 44.27°, 64.42° and 77.47°, which correspond to (111), (200), (220) and (311) Bragg reflections and related to the cubic structure.

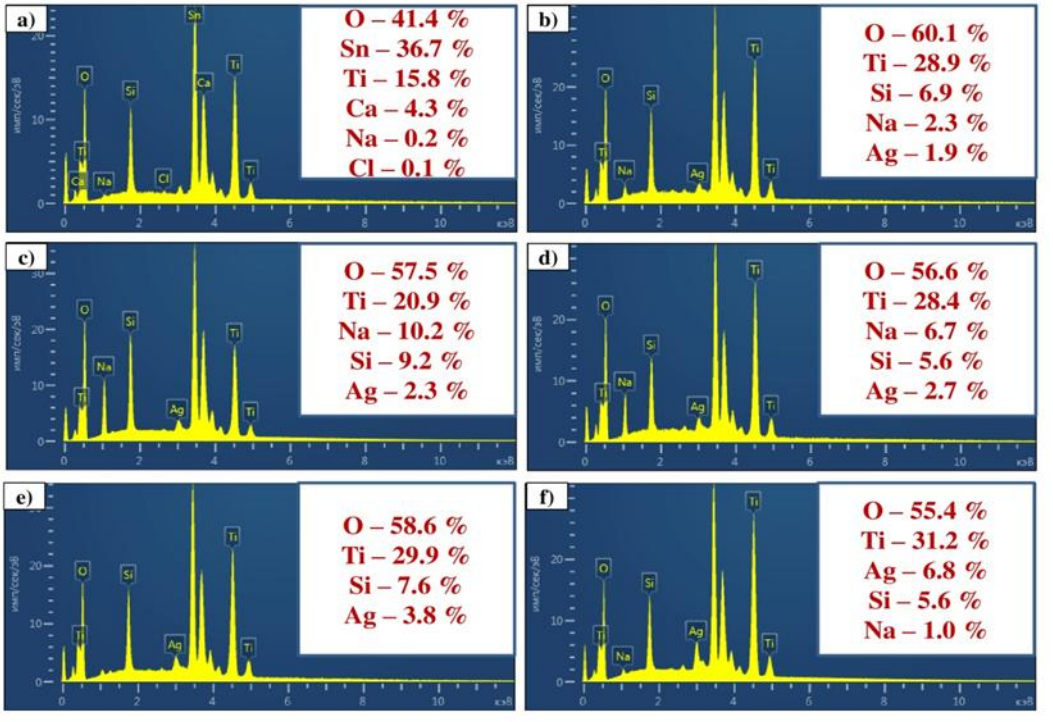

Fig. 2: EDA spectra of TiO2 NRs (a), TAg _0.5 (b), TAg_0.75 (c), TAg_1.0 (d), TAg_1.5 (e), TAg_2.0 (f).

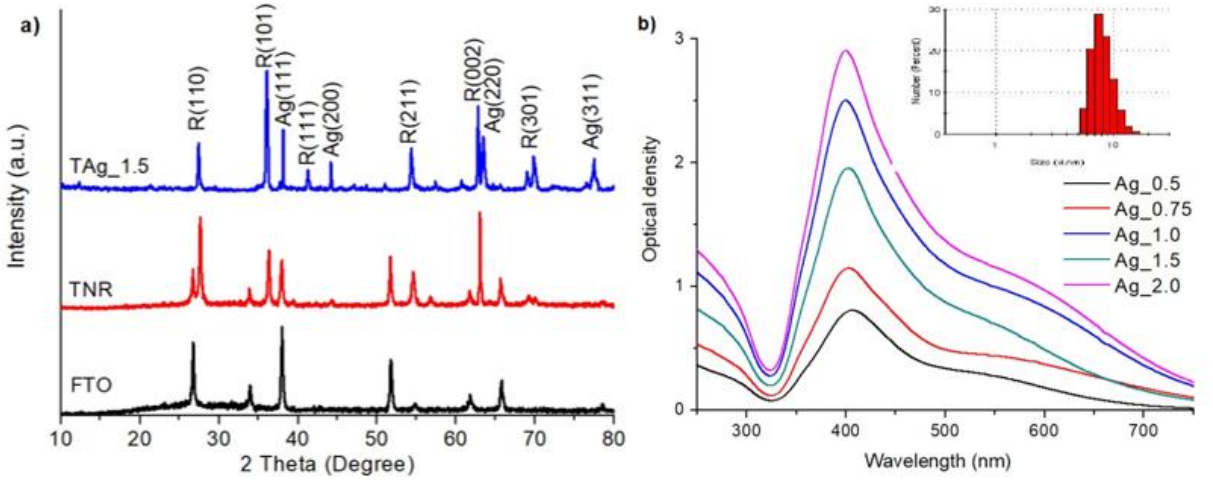

Fig. 3: XRD spectra of TiO_2 nanorods before and after Ag nanoparticle deposition (a), absorption spectra of Ag nanoparticles in solution (b).

The absorption spectra of Ag NPs in H_2O and $C_2H_6O_2$ solutions (1:1 % by volume) is presented at Fig. 3b. As it is known, the absorption spectra of silver NPs depend on their size.[23] The growth in the size of NPs lead to the bathochromic shift of the maximum of the absorption spectrum and to its broadening. Measurements demonstrated that the maximum of the absorption band of Ag NPs exhibits at 408–410 nm for all samples. The dynamic light scattering has shown that Ag NPs have an average diameter of 5 – 12 nm. The largest part of NPs (about 52%) has a diameter of 8 – 9 nm. The data obtained indicate that increasing the amount of $AgNO_3$ in the solution does not result in larger Ag NPs, while the increase in optical density reflects a higher number of NPs in the samples.

The absorption spectrum of TiO_2 NRs without and with deposited Ag NPs (Fig. 4a) demonstrates that the absorption of NRs film exhibits primarily in the UV region of the spectrum, with a maximum at 350 nm. In the presence of Ag NPs, broadening of the absorption of TiO_2 NRs into the visible region is observed, with the appearance of a second absorption band with a maximum at 430 – 450 nm. The observed shift is caused by collective oscillations of electrons on the surface of Ag NPs and corresponds to the absorption of plasmon NPs.

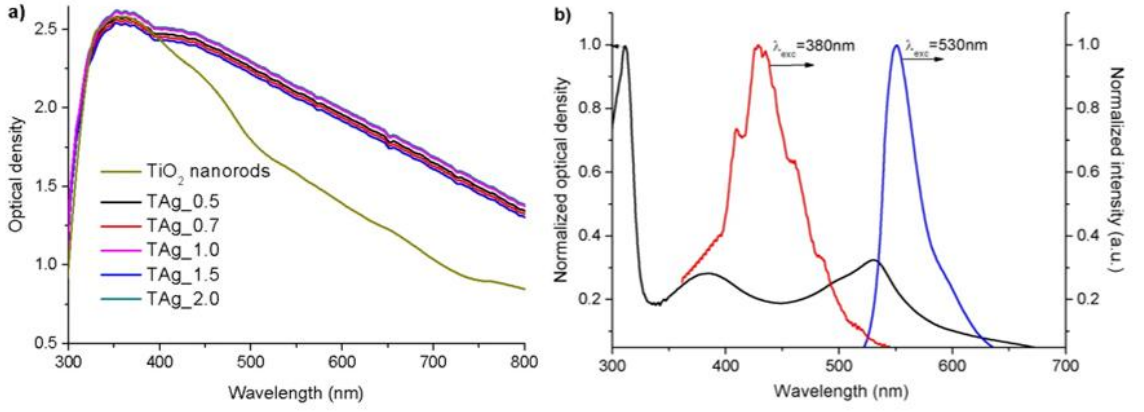

Fig. 4: Absorption spectra of TiO_2 NRs before and after Ag NPs deposition (a) and normalized absorption and fluorescence spectra of N719 dye in ethanol solution (b). The fluorescence spectra of the dye were recorded at different excitation wavelengths (λ_{exc}).

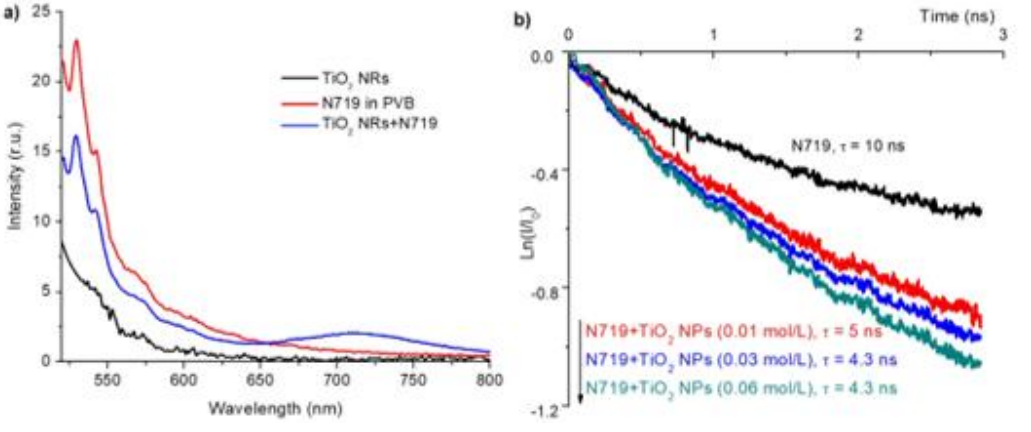

Fig. 5: Fluorescence spectra of N719 molecules in a PVB film and on the surface of TiO_2 NRs doped with dye (a, λ_{exc}=510 nm); the influence of concentration of TiO_2 NPs on the fluorescence decay kinetics of N719 dye in PVB film (b, λ_{reg}=550 nm).

The absorption spectrum of the dye in ethanol (Fig. 4b) is represented by a broad band in the wavelength range of 300 – 650 nm. In the visible region of the spectrum, two bands with maxima at approximately 380 and 530 nm are observed. It is known that the intense absorption band in the region of 300 – 310 nm corresponds to the intramolecular π–π* transition of the bipyridine ligand.[49,50] The band around 380 – 400 nm is the result of ligand-to-ligand charge transfer (LLCT) and metal-to-ligand charge transfer (MLCT), while the band with a maximum at 540 – 550 nm corresponds to low-energy charge transfer between ligands. When the dye molecules were excited at λ_{exc} = 380 nm, the maximum fluorescence band exhibits at 430 nm, and when λ_{exc} = 530 nm, the maximum fluorescence spectrum occurs at 550 nm. In both cases, the emission is caused by relaxation from the MLCT state, which arises as a result of charge transfer from the Ru(II) centre to the π*-orbitals of the bipyridyl ligand.[51,52] Broad emission bands and a distinct Stokes shift (~100 nm) indicate significant geometric changes of molecule in the excited state, which is characteristic of ruthenium complexes with polypyridine ligands.[53,54] Measurements demonstrated that upon adsorption of the dye onto the surface of TiO_2 NRs, as well as upon doping of a polyvinyl butyral (PVB) polymer film with N719 molecules (dye concentration was 10^{-4} mol/L), the absorption and fluorescence spectra of the dye were bathochromically shifted by ~5 – 10 nm. Polymer films were prepared by casting from solution in order to record the fluorescence decay kinetics of dye, which was completely quenched on the surface of TiO_2 NRs.

Fig. 5a presents the emission spectra of dye molecules in PVB and on the surface of TiO_2 NRs. Excitation in the short-wavelength absorption band of the dye (λexc=380 nm) led to the appearance of luminescence from the FTO substrate. Therefore the excitation of the samples was performed with λexc=510 nm. Upon this excitation no luminescence was observed for the samples of neat TiO2 NRs. For samples doped with dye, a decrease in the intensity of dye luminescence was observed. At the same time, along with the dye's fluorescence band with a maximum at 535 nm, a broad emission band was recorded in the 650 – 800 nm range with a maximum at ~720 nm. The recorded luminescence refers to the recombination luminescence of TiO_2 NRs emitted from defect levels located in the band gap of semiconductor.[55] It should be noted that the positions of the luminescence maxima

could be varied depending on the excitation wavelength and the nature of the defects associated with TiO_2 modifications in the form of anatase and rutile. This has been observed previously and discussed in detail in the Ref.[56]

The appearance of recombination luminescence in a semiconductor is the result of charge transfer from the dye to the semiconductor. To confirm this, additional measurements were carried out, where TiO_2 NPs of various concentrations (from 0.01 to 0.06 mol/L) were added to the polymer film with N719. Measurements showed (Fig. 5b) that the decay kinetics of dye fluorescence in the absence of TiO_2 NPs is monoexponential with a lifetime of 10 ns. When the maximal concentration of TiO_2 NPs was added, a 14-fold decrease in dye fluorescence intensity was observed. At the same time, the duration of N719 fluorescence (λreg=550 nm) was decreased to 4.6 ns, or almost ~2.2 times.

It is known that N719 dye molecules have a high yield in the triplet state, from which TiO_2 sensitization also possible.[57] Long-lived luminescence, spectrally coinciding with the spectrum shown in Fig. 5, was observed for the samples of TiO_2 NRs doped with dye molecules. The decay kinetics of the long-lived luminescence of the dye and TiO_2 were recorded at 560 and 720 nm, respectively (Fig. 6a).

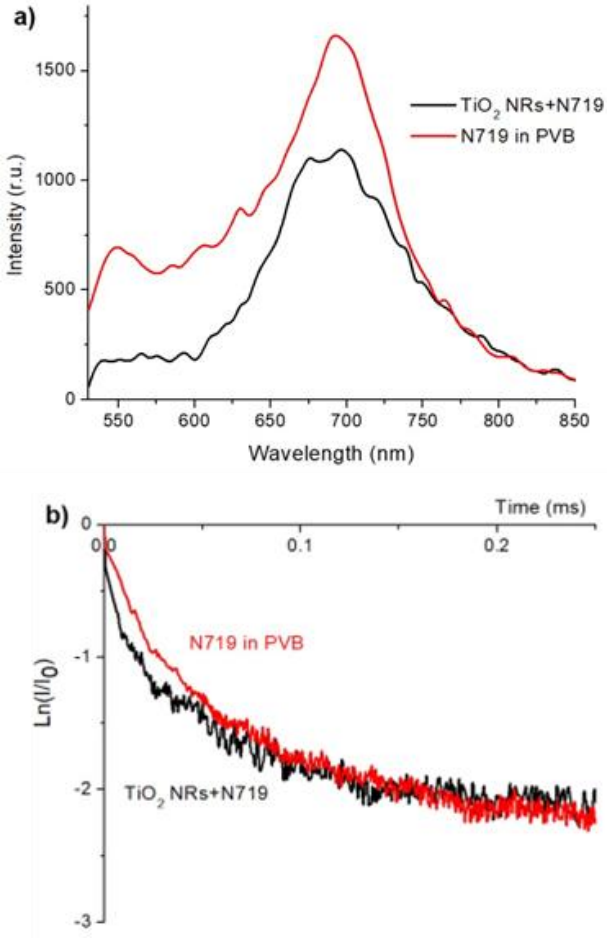

Fig. 6: Spectrum (a) and decay kinetics (b, λ_{reg}=720 nm) of long-lived luminescence of N719 in PVB and on the surface of TiO_2 NRs (λ_{exc}=510 nm).

Measurements revealed that the decay kinetics of long-lived luminescence of N719 in the polymer film is described by a monoexponential function with a lifetime of 127±3 μs at λ_{reg}=560 nm and 98±3 μs at λ_{reg}=720 nm (Table 1). On the contrary, on the surface of the semiconductor, the decay kinetics of the of the dye's long-lived luminescence is biexponential, which indicates the process of charge transfer in the dye/semiconductor system.

Table 1: Lifetime of long-lived luminescence of N719 dye in PVB film and on the surface of TiO_2 NRs (λ_{exc} = 520 nm).

Sample	I	τ_1±3 (μs)	A_1	τ_2±3 (μs)	A_2	<τ>±3 (μs)
N719 in PVB						
λ_{reg}=560 nm	0.1	–	–	–	–	127
λ_{reg}=720 nm	0.2	–	–	–	–	98
TiO_2 NRs+N719						
λ_{reg}=560 nm	32	90	0.25	220	0.75	187
λ_{reg}=720 nm	71	44	0.25	180	0.75	146

Thus, for 560 nm, the lifetime τ_1 of dye luminescence is in 1.4 times shorter than the duration of dye luminescence in a polymer film. For λ_{reg}=720 nm, this parameter reduced by 2.2 times. The appearance of the second component τ_2 is possibly related to the manifestation of recombination luminescence of TiO_2 NRs, therefore the duration of the second component in TiO_2 NRs+N719 samples is higher than in the pure dye film (Fig. 6b).

The efficiency of charge transfer from the dye to the semiconductor was also evaluated from the photovoltaic characteristics of DSSCs based on the prepared films (Fig. 7a). It is seen, that in the absence of Ag NPs, the efficiency of DSSCs is equal to 0.86%, with a short-circuit current density (J_{sc}) of 4.05 mA/cm^2 and an open-circuit voltage (V_{oc}) of 325 mV. The specified efficiency is not a record for DSSCs, since, for greater sorption of dye molecules and their excitation throughout the entire depth, the optimal thickness of the semiconductor layer should be about 10 – 12 μm. In our studies, the thickness of the rods does not exceed 2.6 – 2.7 μm, as the hydrothermal synthesis method does not allow to obtain the films of greater thickness.

However, from the current-voltage characteristics (CVC) of DSSCs it is seen, that the presence of Ag NPs into the structure of the semiconductor layer results in the growth of the efficiency of solar cell (Table 2). Thus, in the TAg_0.5 sample, the J_{sc} is equal to 4.72 mA/cm^2, and the V_{oc} is 373 mV. A further increase in the concentration of precipitated Ag NPs initially leads to an increase in efficiency, followed by a

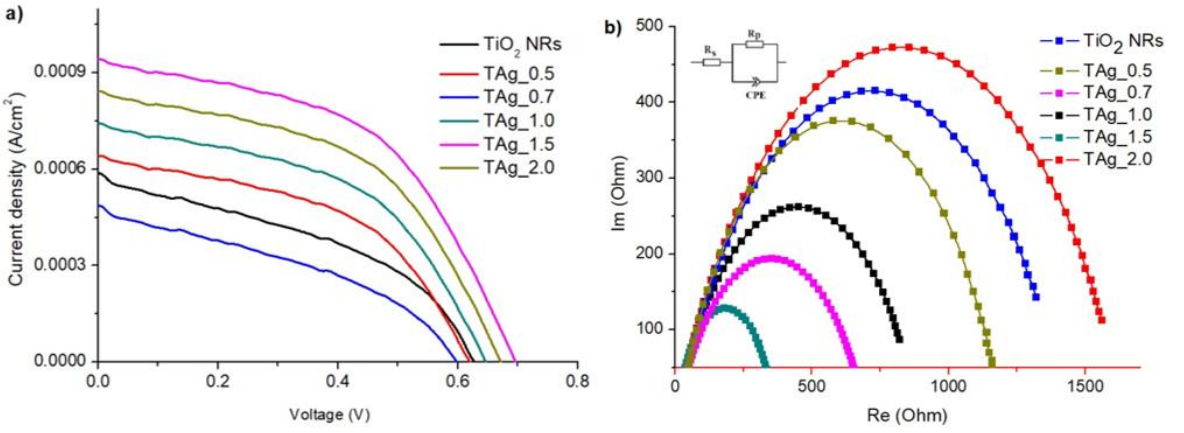

Fig. 7: Current-voltage characteristics (a) and impedance spectra (b) of the DSSCs based on the TiO_2 NRs, doped by N719 dye and Ag NPs.

Table 2: Photovoltaic parameters of DSSCs based on the TiO_2 NRs, doped by N719 dye and Ag NPs.

DSSC type	V_{oc} (mV)	J_{sc} (mA/cm^2)	FF	E_{ff} (%)
TiO_2 NRs + N719	325	4.05	0.30	0.86
TAg_0.5 + N719	373	4.72	0.34	0.92
TAg_0.75 + N719	401	5.42	0.37	1.06
TAg_1.0 + N719	409	5.53	0.31	1.27
TAg_1.5 + N719	691	8.90	0.52	2.72
TAg_2.0 + N719	506	6.52	0.34	1.72

decrease, indicating the presence of an optimal concentration of Ag NPs in the semiconductor. The best photovoltaic parameters were observed for the TAg_1.5 sample where J_{sc} was increased to 8.9 mA/cm^2 and the V_{oc} to 691 mV. The efficiency of the DSSCs based on the TAg_1.5 sample is 2.72%, which is 3.2 times higher than that of the sample without Ag NPs. It is reasonable to assume that the increase in DSSCs efficiency is primarily influenced by the LSPR of Ag NPs, since the thickness of the TiO_2 NRs films is the same and dye molecule adsorption was carried out under identical conditions. Moreover, the experimental data indicate the existence of an optimal concentration of Ag NPs.

The electrochemical impedance spectra in Nyquist coordinates are shown in Fig. 7b and Table 3. The spectra obtained were analysed using the Corrtest Instruments software, and an equivalent circuit consisting of series (R_s) and parallel (R_p) resistances and a constant phase element (CPE). CPE is a constant phase element and represents a capacitive resistance that does not vary on the frequency. According to the theory and methodology described in Ref,[58] Rs characterizes the equivalent resistance to electron transport in TiO_2 and all intercontact layers, while R_p characterizes the resistance to charge carriers transport associated with recombination at the nanocomposite/electrolyte interface. Selecting numerical values for the specified parameters, the impedance spectra of the presented equivalent circuit were selected so that they overlapped with the measured spectra with an error of no more than 0.5%. Further, the effective electron lifetime (τ_{eff}) and recombination rate constant (k_{eff}) were calculated from the hodograph arc.

Calculations have demonstrated that the Rs resistance for all samples was changed when the Ag NPs were deposited. Considering that the total area of all films is 1 cm^2, the observed changes can be attributed only to the presence of Ag NPs. The data presented indicates that as the Ag concentration increases, the film's resistance gradually decreases, and when oversaturation with NPs occurs, it increases again.

Table 3: Numerical values obtained from the calculations of the parameters of the equivalent circuit of DSSCs based on the TiO_2 NRs, doped by N719 dye and Ag NPs.

Sample	R_s (Ohm)	R_p (Ohm)	τ_{eff} (s)	k_{eff} (s^{-1})
TiO_2 + N719	31.7	1386.5	0.11	8.92
TAg_0.5 + N719	30.5	1175.0	0.22	4.46
TAg_0.7 + N719	28.5	820.3	0.23	4.36
TAg_1.0 + N719	27.0	665.8	0.26	3.76
TAg_1.5 + N719	25.3	322.5	0.56	1.78
TAg_2.0 + N719	29.5	1600.6	0,11	9.12

It could be attributed to the effective filling of the semiconductor conduction band with electrons from photoexcited N719 dye molecules under the influence of LSPR of Ag NPs, or to the injection of hot electrons of Ag NPs. Similarly, it can be seen that the effective lifetime of electrons before their recombination increases, while the rate constant decreases, indicating that the LSPR effect of Ag NPs contributes to the effective population of the semiconductor with photoexcited dye electrons.

4. Conclusion

TiO_2 NRs with various concentrations of Ag NPs on their surface were synthesized. The Ag NPs were obtained via a deposition method. According to SEM images, the TiO_2NRs are oriented predominantly perpendicular to the substrate, while the Ag NPs are uniformly distributed across the surface. The size of the deposited NPs ranges from 5 to 12 nm, and they exhibit absorption at 410 nm. Quantitative and qualitative elemental analysis confirmed that an increase in the molar mass of $AgNO_3$ leads to a change in the concentration of deposited Ag NPs from 1.9% to 6.8% relative to the total volume. XRD analysis revealed that the TiO_2 NRs has a tetragonal rutile phase.

The influence of TiO_2 NRs on the spectral and luminescent properties of the N719 dye was studied. It was shown that adsorption of the dye on the surface of TiO_2 NRs leads to a bathochromic shift in both absorption and fluorescence bands. For TiO_2 NRs+ N719 samples, recombination luminescence of the semiconductor was observed, which is attributed to the sensitization of the semiconductor by N719 dye molecules. The addition of TiO_2 NPs to the polymer film of the dye resulted in a 2.2-fold reduction in the fluorescence lifetime of the dye. Moreover, the decrease in the long-lived luminescence lifetime of N719 adsorbed on the TiO_2 NRs surface was also 1.4 – 2.2 times. These results indicate the charge transfer from both singlet and triplet excited states of the N719 dye molecules to TiO_2.

The effect of plasmonic Ag NPs on the sensitization efficiency of TiO_2 NRs with the N719 dye is demonstrated. The TAg_1.5 sample exhibited the highest photoelectric characteristics, showing a 3.2-fold increase in efficiency relative to the Ag NPs-free sample. Impedance measurements indicated that film conductivity increased with Ag NPs loading on the TiO_2 NRs. This may result from effective population of the semiconductor conduction band by electrons from photoexcited N719 molecules facilitated by the Ag NPs; injection of hot electrons generated in the Ag NPs into the TiO_2 conduction band is also possible. A detailed mechanism of the efficiency enhancement in the studied DSSCs will be investigated in our future work. The obtained results demonstrate the potential of using of LSPR of metal NPs to improve the efficiency of solar cells based on semiconductor nanostructures, and may also be applied in the design of high-performance nanophotonic and photovoltaic systems.

Acknowledgments

This work was supported by the Science Committee of the Ministry of Science and Higher Education of the Republic of Kazakhstan [Grant No. AP19680241].

The authors would like to acknowledge the support of the Ministry of Science and Higher Education of the Republic of Kazakhstan under Grant No. BR21882439 ["Advancement of the Green Energy: Foundational Research of Solar Fuel Technologies for Sustainable Production and Advanced Storage"].

Conflict of Interest

There are no conflict to declare.

Supporting Information

Not applicable.

CRediT Statement

G. Omarova: Resources, Investigation, Writing - Original draft, **A. Sadykova:** Investigation, Formal analysis, **T. Serikov:** Methodology, Investigation, Writing - Original draft, **E. Seliverstova:** Visualization, Validation, Writing - Original draft, **N. Ibrayev:** Conceptualization, Methodology, Resources, Writing - Review and editing, **N. Nuraje:** Conceptualization, Writing - Review and editing. The final manuscript was read and approved by all authors.

References

[1] L. Zhang, J. M. Cole, Anchoring groups for dye-sensitized solar cells, *ACS Applied Materials & Interfaces*, 2015, **7**, 3427-3455, doi: 10.1021/am507334m.

[2] S. E. Koops, B. C. O'Regan, P. R. F. Barnes, J. R. Durrant, Parameters influencing the efficiency of electron injection in dye-sensitized solar cells, *Journal of the American Chemical Society*, 2009, **131**, 4808-4818, doi: 10.1021/ja8091278.

[3] J. Gong, K. Sumathy, Q. Qiao, Z. Zhou, Review on dye-sensitized solar cells (DSSCs): advanced techniques and research trends, *Renewable and Sustainable Energy Reviews*, 2017, **68**, 234-246, doi: 10.1016/j.rser.2016.09.097.

[4] J. E. Ikpesu, S. E. Iyuke, M. Daramola, A. O. Okewale, Synthesis of improved dye-sensitized solar cell for renewable energy power generation, *Solar Energy*, 2020, **206**, 918-934, doi: 10.1016/j.solener.2020.05.002.

[5] A. Pallikkara, K. Ramakrishnan, Efficient charge collection of photoanodes and light absorption of photosensitizers: a review, *International Journal of Energy Research*, 2021, **45**, 1425-1448, doi: 10.1002/er.5941.

[6] C. Biswas, M. S. Ahmed, S. S. K. Raavi, Ultrafast electron injection kinetics and effect of plasmonic silver nanoparticle at organic dye-TiO_2 interface, *Asian Journal of Physics*, 2021, **30**, 933, doi: 10.54955/ajp.30.6.2021.933-945.

[7] A. Listorti, B. O'Regan, J. R. Durrant, Electron transfer dynamics in dye-sensitized solar cells, *Chemistry of Materials*, 2011, **23**, 3381-3399, doi: 10.1021/cm200651e.

[8] Z. Chen, F. Li, C. Huang, Organic D-π-a dyes for dye-sensitized solar cell, *Current Organic Chemistry*, 2007, **11**, 1241-1258, doi: 10.2174/138527207781696008.
[9] S. G. Bairu, E. Mghanga, J. Hasan, S. Kola, V. J. Rao, K. Bhanuprakash, L. Giribabu, G. P. Wiederrecht, R. da Silva, L. G. C. Rego, G. Ramakrishna, Ultrafast interfacial charge-transfer dynamics in a donor-π-acceptor chromophore sensitized TiO_2 nanocomposite, *The Journal of Physical Chemistry C*, 2013, **117**, 4824-4835, doi: 10.1021/jp310642t.
[10] A. Demir, F. Aslan, H. Esen, TiO_2/ZnO-based composite thin films coated on FTO surface by screen printing method: increasing dye-sensitized solar cell performance, *Journal of Materials Science*: *Materials in Electronics*, 2024, **35**, 1481, doi: 10.1007/s10854-024-13213-z.
[11] A. Banik, M. S. Ansari, M. Qureshi, Efficient energy harvesting in SnO_2-based dye-sensitized solar cells utilizing nano-amassed mesoporous zinc oxide hollow microspheres as synergy boosters, *ACS Omega*, 2018, **3**, 14482-14493, doi: 10.1021/acsomega.8b02520.
[12] N. K. Elumalai, C. Vijila, R. Jose, A. Uddin, S. Ramakrishna, Metal oxide semiconducting interfacial layers for photovoltaic and photocatalytic applications, *Materials for Renewable and Sustainable Energy*, 2015, **4**, 11, doi: 10.1007/s40243-015-0054-9.
[13] B. Pari, S. Chidambaram, N. Kasi, S. Muthusamy, Recent advances in SnO_2 based photo anode materials for third generation photovoltaics, *Materials Science Forum*, 2013, **771**, 25-38, doi: 10.4028/www.scientific.net/msf.771.25.
[14] P. Tiwana, P. Docampo, M. B. Johnston, H. J. Snaith, L. M. Herz, Electron mobility and injection dynamics in mesoporous ZnO, SnO_2, and TiO_2 films used in dye-sensitized solar cells, *ACS Nano*, 2011, **5**, 5158-5166, doi: 10.1021/nn201243y.
[15] B. O'Regan, M. Grätzel, A low-cost, high-efficiency solar cell based on dye-sensitized colloidal TiO_2 films, *Nature*, 1991, **353**, 737-740, doi: 10.1038/353737a0.
[16] X. Feng, K. Zhu, A. J. Frank, C. A. Grimes, T. E. Mallouk, Rapid charge transport in dye-sensitized solar cells made from vertically aligned single-crystal rutile TiO_2 nanowires, *Angewandte Chemie* (*International Ed*), 2012, **51**, 2727-2730, doi: 10.1002/anie.201108076.
[17] J. Wang, Z. Lin, Dye-sensitized TiO_2 nanotube solar cells: rational structural and surface engineering on TiO_2 nanotubes, *Chemistry – An Asian Journal*, 2012, **7**, 2754-2762, doi: 10.1002/asia.201200349.
[18] T. M. Serikov, The effect of electric transport properties of titanium dioxide nanostructures on their photocatalytic activity, *Bulletin of the Karaganda University \"Physics Series\"*, 2020, **99**, 13-21, doi: 10.31489/2020ph3/13-21.
[19] P. Poudel, Q. Qiao, One dimensional nanostructure/nanoparticle composites as photoanodes for dye-sensitized solar cells, *Nanoscale*, 2012, **4**, 2826, doi: 10.1039/c2nr30347g.
[20] J. Maçaira, L. Andrade, A. Mendes, Review on nanostructured photoelectrodes for next generation dye-sensitized solar cells, *Renewable and Sustainable Energy Reviews*, 2013, **27**, 334-349, doi: 10.1016/j.rser.2013.07.011.
[21] M. Lv, D. Zheng, M. Ye, J. Xiao, W. Guo, Y. Lai, L. Sun, C. Lin, J. Zuo, Optimized porous rutile TiO_2 nanorod arrays for enhancing the efficiency of dye-sensitized solar cells, *Energy & Environmental Science*, 2013, **6**, 1615-1622, doi: 10.1039/C3EE24125D.
[22] K. Sharma, V. Sharma, S. S. Sharma, Dye-sensitized solar cells: fundamentals and current status, *Nanoscale Research Letters*, 2018, **13**, 381, doi: 10.1186/s11671-018-2760-6.
[23] D. Ghernaout, A. Boudjemline, N. Elboughdiri, Electrochemical engineering in the core of the dye-sensitized solar cells (DSSCs), *OALib*, 2020, **7**, 1-12, doi: 10.4236/oalib.1106178.
[24] K. Kakiage, Y. Aoyama, T. Yano, K. Oya, J.-I. Fujisawa, M. Hanaya, Highly-efficient dye-sensitized solar cells with collaborative sensitization by silyl-anchor and carboxy-anchor dyes, *Chemical Communications*, 2015, **51**, 15894-15897, doi: 10.1039/C5CC06759F.
[25] F. D'Amico, B. D. Jong, M. Bartolini, D. Franchi, A. Dessì, L. Zani, X. Yzeiri, E. Gatto, A. Santucci, A. Di Carlo, G. Reginato, L. Cinà, L. Vesce, Recent advances in organic dyes for application in dye-sensitized solar cells under indoor lighting conditions, *Materials*, 2023, **16**, 7338, doi: 10.3390/ma16237338.
[26] M. Kokkonen, P. Talebi, J. Zhou, S. Asgari, S. A. Soomro, F. Elsehrawy, J. Halme, S. Ahmad, A. Hagfeldt, S. G. Hashmi, Advanced research trends in dye-sensitized solar cells, *Journal of Materials Chemistry A*, 2021, **9**, 10527-10545, doi: 10.1039/d1ta00690h.
[27] E. Kouhestanian, S. Ahmad Mozaffari, M. Ranjbar, H. S. Amoli, Enhancing the electron transfer process of TiO_2-based DSSC using DC magnetron sputtered ZnO as an efficient alternative for blocking layer, *Organic Electronics*, 2020, **86**, 105915, doi: 10.1016/j.orgel.2020.105915.
[28] L. Wei, X. Xia, Y. Yang, P. Wang, Y. Dong, T. Luan, Variable temperature spectroelectrochemistry study of silver-doped TiO_2 and its influence on the performance of dye sensitized solar cells, *RSC Advances*, 2016, **6**, 68341-68350, doi: 10.1039/C6RA10747H.
[29] E. H. Onah, N. L. Lethole, P. Mukumba, Luminescent materials for dye-sensitized solar cells: advances and directions, *Applied Sciences*, 2024, **14**, 9202, doi: 10.3390/app14209202.
[30] N. F. M. Sharif, M. Z. A. A. Kadir, S. Shafie, S. A. Rashid, W. Z. Wan Hasan, S. Shaban, Charge transport and electron recombination suppression in dye-sensitized solar cells using graphene quantum dots, *Results in Physics*, 2019, **13**, 102171, doi: 10.1016/j.rinp.2019.102171.
[31] D. Joshy, S. B. Narendranath, Y. A. Ismail, P. Periyat, Recent progress in one dimensional TiO_2 nanomaterials as photoanodes in dye-sensitized solar cells, *Nanoscale Advances*, 2022, **4**, 5202-5232, doi: 10.1039/D2NA00437B.
[32] P. S. Saud, A. Bist, A. A. Kim, A. Yousef, A. Abutaleb, M. Park, S.-J. Park, B. Pant, Dye-sensitized solar cells: fundamentals, recent progress, and optoelectrical properties improvement strategies, *Optical Materials*, 2024, **150**, 115242, doi: 10.1016/j.optmat.2024.115242.

[33] Masud, H. K. Kim, Redox shuttle-based electrolytes for dye-sensitized solar cells: comprehensive guidance, recent progress, and future perspective, *ACS Omega*, 2023, **8**, 6139-6163, doi: 10.1021/acsomega.2c06843.
[34] Y. Xin, K. Yu, L. Zhang, Y. Yang, H. Yuan, H. Li, L. Wang, J. Zeng, Copper-based plasmonic catalysis: recent advances and future perspectives, *Advanced Materials*, 2021, **33**, 2008145, doi: 10.1002/adma.202008145.
[35] Q. Duan, Y. Liu, S. Chang, H. Chen, J.-H. Chen, Surface plasmonic sensors: sensing mechanism and recent applications, *Sensors*, 2021, **21**, 5262, doi: 10.3390/s21165262.
[36] E. Seliverstova, T. Serikov, N. Nuraje, N. Ibrayev, A. Sadykova, M. Amze, Plasmonic effect of metal nanoparticles on the photocatalytic properties of TiO_2/rGO composite, *Nanotechnology*, 2024, **35**, 325401, doi: 10.1088/1361-6528/ad3e02.
[37] T. M. Serikov, P. A. Zhanbirbayeva, A. S. Baltabekov, A. B. Kuanyshbekova, Photocatalytic activity of the TIO2/Ag/rGO nanocomposite, *Bulletin of the Karaganda University \"Physics Series\"*, 2022, **108**, 14-21, doi: 10.31489/2022ph4/14-21.
[38] J. Li, Z. Lou, B. Li, Nanostructured materials with localized surface plasmon resonance for photocatalysis, *Chinese Chemical Letters*, 2022, **33**, 1154-1168, doi: 10.1016/j.cclet.2021.07.059.
[39] T. M. Serikov, A. S. Kayumova, A. S. Baltabekov, L. F. Ilyina, P. A. Zhanbirbayeva, Photocatalytic activity of nanocomposites based on titania nanorods and nanotubes doped with Ag and reduced graphene oxide nanoparticles, *Nanobiotechnology Reports*, 2023, **18**, 207-215, doi: 10.1134/s2635167623700040.
[40] G. V. Belessiotis, A. G. Kontos, Plasmonic silver (Ag)-based photocatalysts for H_2 production and CO_2 conversion: review, analysis and perspectives, *Renewable Energy*, 2022, **195**, 497-515, doi: 10.1016/j.renene.2022.06.044.
[41] E. Seliverstova, N. Ibrayev, G. Omarova, A. Ishchenko, M. Kucherenko, Competitive influence of the plasmon effect and energy transfer between chromophores and Ag nanoparticles on the fluorescent properties of indopolycarbocyanine dyes, *Journal of Luminescence*, 2021, **235**, 118000, doi: 10.1016/j.jlumin.2021.118000.
[42] X. Li, W. Yang, J. Deng, Y. Lin, Surface plasmon resonance effects of silver nanoparticles in graphene-based dye-sensitized solar cells, *Frontiers in Materials*, 2023, **10**, 1137771, doi: 10.3389/fmats.2023.1137771.
[43] A. Razaghizadeh, V. Rafee, R. Nakhaei, F. Ameri, Effect of silver nanoparticles embedding in mesoporous TiO_2 layer on the performance enhancement of dye-sensitized solar cells using natural dyes, *Plasmonics*, 2025, **20**, 7951-7965, doi: 10.1007/s11468-025-02836-5.
[44] L. S. Daniel, R. T. Kaffer, L. M. Kalipi, A. Rahman, M. Kalengay, V. Uahengo, The photon-electrical conversion efficiency of dye-sensitive solar cells fabricated using a highly conductive silver-nanoparticle/titania photocathode, *Applied Research*, 2024, **3**, e202300044, doi: 10.1002/appl.202300044.
[45] S. Shah, Z. H. Z. Abidin, I. M. Noor, Z. Osman, A. K. Arof, Performance improvement of dye-sensitized solar cells with Ag nanoparticles, *Molecular Crystals and Liquid Crystals*, 2023, **762**, 88-98, doi: 10.1080/15421406.2023.2180213.
[46] V. S. Manikandan, A. K. Palai, A. Ramadoss, S. Mohanty, M. Navaneethan, Plasmon enfolded TiO_2 hierarchical photoanode: fabrication and the performance evaluation as liquid-based dye-sensitized solar cell, *Journal of Materials Science: Materials in Electronics*, 2022, **33**, 8655-8664, doi: 10.1007/s10854-021-06724-6.
[47] T. M. Serikov, N. K. Ibrayev, T. M. Ivanova, S. V. Savilov, Influence of the hydrothermal synthesis conditions on the photocatalytic activity of titanium dioxide nanorods, *Russian Journal of Applied Chemistry*, 2021, **94**, 442-449, doi: 10.1134/S1070427221040030.
[48] T. M. Serikov, A. S. Kayumova, A. S. Baltabekov, L. F. Ilyina, P. A. Zhanbirbayeva, Photocatalytic activity of nanocomposites based on titania nanorods and nanotubes doped with Ag and reduced graphene oxide nanoparticles, *Nanobiotechnology Reports*, 2023, **18**, 207-215, doi: 10.1134/S2635167623700040.
[49] A. El-Shafei, M. Hussain, A. Atiq, A. Islam, L. Han, A novel carbazole-based dye outperformed the benchmark dye N719 for high efficiency dye-sensitized solar cells (DSSCs), *Journal of Materials Chemistry*, 2012, **22**, 24048-24056, doi: 10.1039/C2JM35267B.
[50] F. De Angelis, S. Fantacci, E. Mosconi, M. K. Nazeeruddin, M. Grätzel, Absorption spectra and excited state energy levels of the N719 dye on TiO_2 in dye-sensitized solar cell models, *The Journal of Physical Chemistry C*, 2011, **115**, 8825-8831, doi: 10.1021/jp111949a.
[51] N. H. Damrauer, G. Cerullo, A. Yeh, T. R. Boussie, C. V. Shank, J. K. McCusker, Femtosecond dynamics of excited-state evolution in $[Ru(bpy)_3]^{2+}$, *Science*, 1997, **275**, 54-57, doi: 10.1126/science.275.5296.54.
[52] M.-A. Haga, M. M. Ali, H. Maegawa, K. Nozaki, A. Yoshimura, T. Ohno, Photoexcited states of dinuclear Ru complexes bridged by proton-dissociable benzimidazole derivatives, *Coordination Chemistry Reviews*, 1994, **132**, 99-104, doi: 10.1016/0010-8545(94)80028-6.
[53] J. P. Sauvage, J. P. Collin, J. C. Chambron, S. Guillerez, C. Coudret, V. Balzani, F. Barigelletti, L. De Cola, L. Flamigni, Ruthenium(II) and osmium(II) bis(terpyridine) complexes in covalently-linked multicomponent systems: synthesis, electrochemical behavior, absorption spectra, and photochemical and photophysical properties, *Chemical Reviews*, 1994, **94**, 993-1019, doi: 10.1021/cr00028a006.
[54] K. M. Lancaster, J. B. Gerken, A. C. Durrell, J. H. Palmer, H. B. Gray, Electronic structures, photophysical properties, and electrochemistry of ruthenium(II)$(bpy)_2$ pyridylimidazole complexes, *Coordination Chemistry Reviews*, 2010, **254**, 1803-1811, doi: 10.1016/j.ccr.2010.04.005.
[55] M. Rajabi, S. Shogh, A. Iraji zad, Defect study of TiO_2 nanorods grown by a hydrothermal method through photoluminescence spectroscopy, *Journal of Luminescence*, 2015, **157**, 235-242, doi: 10.1016/j.jlumin.2014.08.035.
[56] V. M. Ievlev et al., Luminescence of titanium dioxide thin films, *Kondensirovannye sredy i mezhfaznye granitsy*, 2012, **14**(2), 141-149.

[57] S. K. Vemula, S. M. Chelli, C. Biswas, V. R. Soma, S. S. K. Raavi, Adsorption and electron injection studies in N719 sensitized Ag −, Au − implanted and O_2 annealed titania films, *Optical Materials*, 2024, **154**, 115633, doi: 10.1016/j.optmat.2024.115633.
[58] M. Adachi, M. Sakamoto, J. Jiu, Y. Ogata, S. Isoda, Determination of parameters of electron transport in dye-sensitized solar cells using electrochemical impedance spectroscopy, *The Journal of Physical Chemistry. B*, 2006, **110**, 13872-13880, doi: 10.1021/jp061693u.

Publisher's Note: Engineered Science Publisher remains neutral with regard to jurisdictional claims in published maps and institutional affiliations.

Open Access
This article is licensed under a Creative Commons Attribution 4.0 International License, which permits the use, sharing, adaptation, distribution and reproduction in any medium or format, as long as appropriate credit to the original author(s) and the source is given by providing a link to the Creative Commons license and changes need to be indicated if there are any. The images or other third-party material in this article are included in the article's Creative Commons license, unless indicated otherwise in a credit line to the material. If material is not included in the article's Creative Commons license and your intended use is not permitted by statutory regulation or exceeds the permitted use, you will need to obtain permission directly from the copyright holder. To view a copy of this license, visit http://creativecommons.org/ licenses/by/4.0/.

©The Author(s) 2025.